

# Two-dimensional apodized silicon photonic phased arrays

Jie Sun,<sup>1,\*</sup> Ehsan shah Hosseini,<sup>1</sup> Ami Yaacobi,<sup>1</sup> David B. Cole,<sup>1</sup> Gerald Leake,<sup>2</sup>  
Douglas Coolbaugh,<sup>2</sup> and Michael R. Watts<sup>1</sup>

<sup>1</sup>Research Laboratory of Electronics, Massachusetts Institute of Technology, Cambridge, Massachusetts 02139, USA

<sup>2</sup>College of Nanoscale Science and Engineering, University at Albany, Albany, New York 12203, USA

\*Corresponding author: sunjie@mit.edu

Received October 28, 2013; revised December 8, 2013; accepted December 15, 2013;  
posted December 16, 2013 (Doc. ID 200207); published January 15, 2014

In this Letter, we demonstrate an  $8 \times 8$  apodized silicon photonic phased array where the emission from each of 64 nanoantennas was tailored to exhibit Gaussian-shaped intensity distributions in the near field so that the sidelobes of the generated far-field optical beam were suppressed compared to that of a uniform phased array. With the aid of the 72 thermo-optic phase tuners directly integrated within the phased array, we dynamically shaped the generated optical beam in the far field in a variety of ways. © 2014 Optical Society of America

OCIS codes: (130.3120) Integrated optics devices; (250.3140) Integrated optoelectronic circuits; (280.5110) Phased-array radar.

<http://dx.doi.org/10.1364/OL.39.000367>

Optical phased arrays, for optical beam forming and beam steering, are poised to enable applications from optical communication through laser radar (ladar) to optical sensing [1]. Having been studied for decades, optical phased arrays take many forms, from laser arrays [2], to liquid crystals [3], to microelectromechanical systems [4,5]. Combined with complementary metal-oxide-semiconductor technologies, optical phased arrays have been developed in integrated form using silicon photonic circuits [6–8], an approach of particular interest for its promise of large-scale integration. As a step forward, we recently demonstrated such a large-scale silicon photonic phased array capable of projecting arbitrary holographic images in the far field [9]. In all of these silicon photonic phased arrays, the far-field beam forms are generated solely by engineering the phase of the optical antennas while the amplitude of the optical emission across the antenna array is kept uniform. However, phase control alone does not provide complete control of the optical field. Indeed amplitude control must also be incorporated to enable truly arbitrary far-field distributions [10]. Here we show, with our previously demonstrated phased array architecture [9], the amplitude distribution of the optical emission in the phased array can also be tailored to shape the far-field optical beam form. In particular, we demonstrate an  $8 \times 8$  silicon photonic phased array where the amplitude of the optical emission is apodized with a Gaussian distribution to suppress the sidelobes that normally present in optical phased arrays with uniform amplitude; in addition, we show that the generated optical beam can be actively manipulated in various ways by use of the 72 thermo-optic tunable phase shifters that are directly integrated within the phased array.

In an  $M \times N$  optical phased array, the far-field radiation profile  $F_a(\theta, \phi)$ , formed by the interference of a large number of optical antennas, is related to its near-field emission profile by the Fourier transform (denoted by “ $\mathcal{F}$ ”) [11]:

$$F_a(\theta, \phi) \sim \mathcal{F}(w_{mn}) = \mathcal{F}(A_{mn} \cdot e^{j\varphi_{mn}}), \quad (1)$$

where  $(m, n)$  is the array index of the individual antenna, and  $w_{mn}$  is the near-field emission profile that contains both the amplitude ( $A_{mn}$ ) and phase ( $\varphi_{mn}$ ). According to the Fourier relation, a uniform phased array that has an unvarying rectangular amplitude profile across the array [as shown in Fig. 1(a)] generates a sinc-like beam form in the far field with sidelobes, as simulated in Fig. 1(b). It is seen in Fig. 1(b) that multiple interference orders appear in the far field, because the antennas are spaced by multiple times of the operating wavelength. Also note that the intensities of the interference orders differ from one another, with a distribution corresponding to the far-field radiation profile of the individual optical antenna [9]. Sidelobes arise in each order and are more evident in the orders of greatest intensity, as shown in the upper part of Fig. 1(b). For most applications, it is

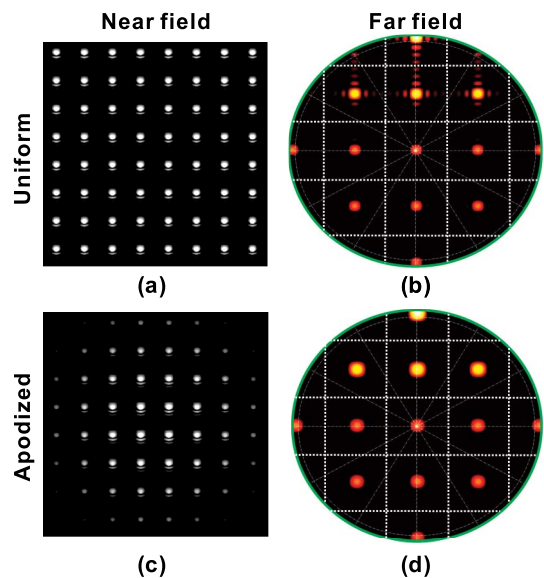


Fig. 1. Simulated (a) near-field emission and (b) far-field optical beam form of a uniform  $8 \times 8$  phased array. Simulated (c) near-field emission and (d) far-field optical beam form of a Gaussian-apodized  $8 \times 8$  phased array.

desirable to suppress these unwanted sidelobes to enhance the overall performance of the phased array. This can be done by apodization; that is, the amplitude profile is trimmed by some nonuniform window function. For example, Fig. 1(c) illustrates an apodized  $8 \times 8$  optical phased array with a Gaussian window where the emission amplitude of the optical antennas decays from the center to the edge of the array, following a Gaussian distribution. Figure 1(d) simulates the corresponding far-field beam form of the apodized phased array where the sidelobes are successfully suppressed in every order. The calculated sidelobe level is  $-25$  dB. It is also seen that the size of the beam is expanded in the apodized array, a consequence of the reduced effective array area due to the apodization.

The challenge of building an apodized optical phased array lies in the difficulty of accurately feeding each optical antenna with the precise amount of optical power to form a desired amplitude apodization profile, a challenge that cannot be surmounted by previous silicon photonic phased array architectures, especially in large-scale arrays. It can, however, be well addressed by our recently developed large-scale optical phased array architecture, where the optical nanoantennas are precisely fed by a series of directional couplers [9]. Figure 2(a) illustrates the architecture of an  $8 \times 8$  optical phased array consisting of 64 antenna unit cells  $9 \mu\text{m}$  apart from each other in both directions. As shown in the inset of Fig. 2(a), each unit cell is composed of a compact dielectric optical nanoantenna, a thermo-optically tunable optical delay line formed by doping the silicon waveguide, and a directional coupler with length  $L_{mn}$ . There are also another 8 directional couplers that couple light from the main bus waveguide to the 8 row waveguides. The coupling coefficients of the 72 directional couplers can be adjusted through the coupler length so as to achieve any desired amplitude profile in the phased array. Figure 2(b) calculates the coupling coefficients of the 72 directional couplers in order to realize the Gaussian-shaped apodization shown in Fig. 1(c). The corresponding coupler lengths were calculated in Fig. 2(c) using a rigorous 3D finite difference time-domain (FDTD) simulation. The coupler length varies from  $0.52$  to  $4.7 \mu\text{m}$  to cover a range of coupling coefficients from  $2.6\%$  to  $59\%$ . The width of the silicon waveguides is  $0.4 \mu\text{m}$  and the gap between the waveguide and the directional coupler is  $0.12 \mu\text{m}$ . The designed apodized  $8 \times 8$  optical phased array was fabricated in a  $300 \text{ nm}$  silicon-on-insulator process using  $193 \text{ nm}$  optical immersion lithography. Two levels of  $n$ -type doping were implanted to form a silicon resistor in each unit cell where the silicon waveguide is directly heated to provide the most power-efficient thermo-optic tuning [12]. A uniform  $8 \times 8$  optical phased array was also fabricated on the same chip for comparison. Figure 2(d) shows an optical micrograph of the fabricated apodized phased array, while the inset shows a scanning-electron micrograph (SEM) of the optical nanoantenna. Figure 2(e) shows an SEM of the fabricated phased array, which was taken by dry etching away the dielectric  $\text{SiO}_2$  using the metal layers as a hard mask.

The fabricated uniform and apodized  $8 \times 8$  optical phased arrays were tested by coupling a  $1.55 \mu\text{m}$  laser from a single-mode fiber into the silicon bus waveguide

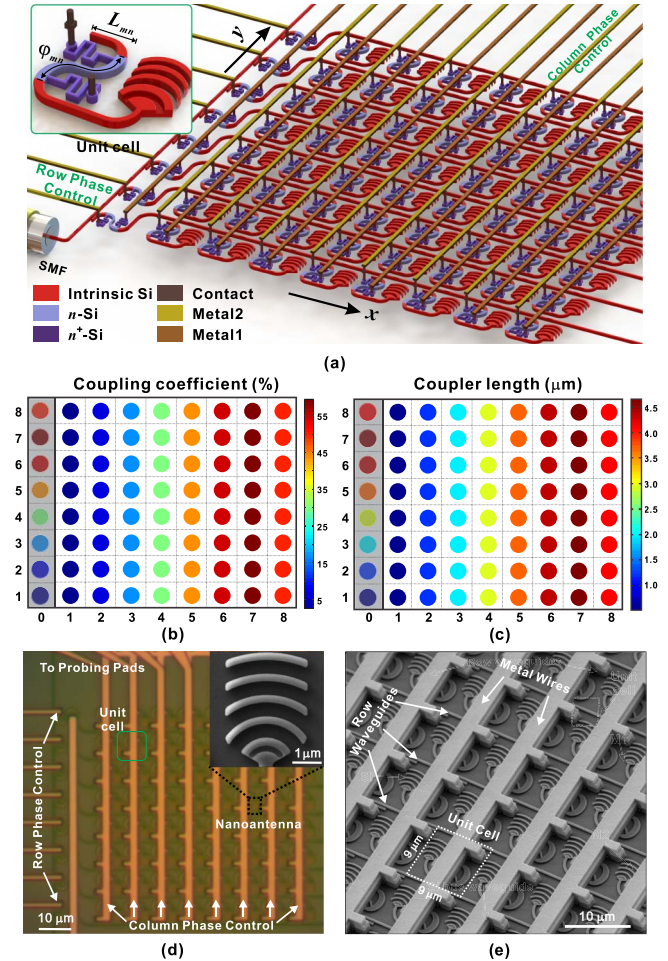


Fig. 2. (a) Schematics of the silicon photonic phased array. Inset: a unit cell ( $m, n$ ) of the phased array, including a directional coupler of length  $L_{mn}$ , a thermo-optically tunable optical delay line for a delayed phase  $\varphi_{mn}$ , and a compact optical nanoantenna. (b) The coupling coefficients of the 72 directional couplers to realize a Gaussian apodization profile. (c) The corresponding length of the directional couplers calculated from rigorous 3D FDTD. The shaded column corresponds to the 8 directional couplers that couple light from the main bus waveguide to the 8 row waveguides. (d) An optical image of the fabricated  $8 \times 8$  apodized phased array. Inset: an SEM of the optical nanoantenna. (e) An SEM of the fabricated array after dry etching away the dielectric  $\text{SiO}_2$ .

with a transverse-electric polarization. The phase profile was set by design as  $\varphi_{mn} = 0$  when no thermo-optic tuning is applied. The near-field and far-field images were taken with the same setup described in [9], using an objective with a numerical aperture of  $0.4$  ( $\text{NA} = 0.4$ ). Figure 3(a) shows the measured near-field emission of the uniform array where each optical antenna emits with the same amplitude. Similar to the simulations in Fig. 1(b), sidelobes appear in the far field especially in the interference orders with high intensity, as shown in Fig. 3(b). By comparison, Figs. 3(c) and 3(d) show the measured near-field emission and far-field beam form of the apodized phased array. Figure 3(c) reveals that the designed amplitude apodization was achieved, where the emission amplitude decreases from the center to the edge of the array. Note that not all of the 64 optical antennas are seen in Fig. 3(c) because some antennas

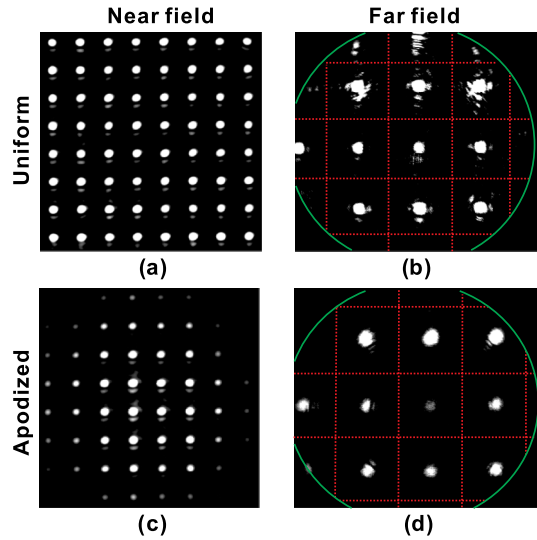


Fig. 3. Measured (a) near-field emission and (b) far-field optical beam form of a uniform  $8 \times 8$  phased array. Measured (c) near-field emission and (d) far-field optical beam form of a Gaussian-apodized  $8 \times 8$  phased array.

on the edge are too dim to be captured by the infrared camera. Accordingly, the sidelobes were successfully suppressed thanks to the amplitude apodization, as shown in Fig. 3(d). The measured sidelobe level is about  $-19$  dB. According to the Fourier relation in Eq. (1), each of the interference orders in Fig. 3(d) contains a Gaussian-shaped optical beam with a measured beam width about  $1.6^\circ$ . Note that the green circles in Fig. 3 as well as in the simulations in Fig. 1 correspond to a view field  $\theta \leq 24^\circ$ , set by the numerical aperture of the objective. The good agreement between the experiment (Fig. 3) and the simulation (Fig. 1) in both near field and far field confirms the accuracy and reliability of the silicon photonic design and fabrication, as well as the high tolerance of phased arrays to phase and intensity noises [13]. Note that the center interference order in Fig. 3(d) is dimmer, indicating that the single antenna radiation of the fabricated apodized array has a local minimum around the zenith of the far field [i.e., the center of Fig. 3(d)].

By applying different voltages on each unit cell, the phase profile  $\varphi_{mn}$  of the apodized array can be modified through the thermo-optic effect, resulting in dynamic beam manipulation in the far field. Figure 4 shows a variety of optical beam forms generated by the apodized array through reconfiguring the phase profile. Figure 4(a) shows the reference beam when no voltage was applied, where a Gaussian-shaped beam is observed in one of the interference orders in the far field. This Gaussian-shaped beam can be actively steered in two dimensions [Fig. 4(b)], split into a  $1 \times 2$  beam array [Fig. 4(c)], split into a  $2 \times 1$  beam array and shifted at the same time [Fig. 4(d)], and split into a  $2 \times 2$  beam array [Fig. 4(e)]. The corresponding phase profiles and simulated beam forms are also shown in Fig. 4. Again good agreement between simulation and measurement is observed. The measured tuning efficiency of the thermo-optic phase shifter is  $\sim 8.5$  mW per  $\pi$  phase shift for each unit cell, which could be further improved using, for example, local substrate removal that provides a better thermal insulation [14].

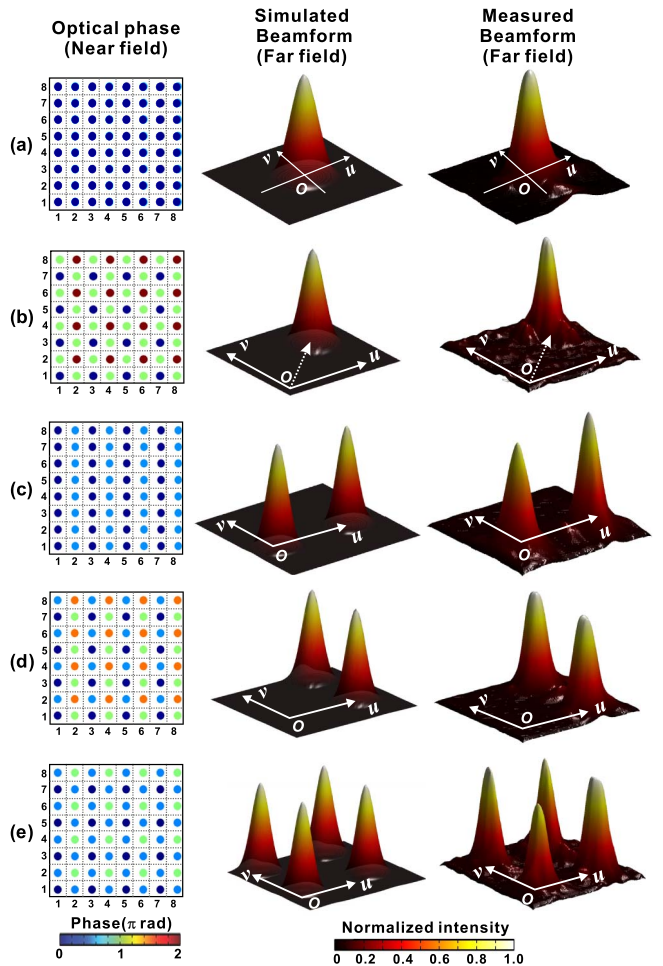


Fig. 4. Dynamic beam form generation using the apodized phased array. (a) The reference beam form with no phase tuning. The optical beam in the far field is (b) steered, (c) split into a  $1 \times 2$  beam array, (d) split into a  $2 \times 1$  beam array and shifted, and (e) split into a  $2 \times 2$  beam array with active phase tuning. Note that only one of the interference orders in the far field is shown here.

In this Letter, we demonstrated an  $8 \times 8$  optical phased array with Gaussian-apodized amplitude profile to suppress the sidelobes of the far-field beam form. The demonstrated ability to simultaneously engineer both the amplitude and phase profile in a large-scale 2D silicon photonic phased array enables arbitrary optical beam forms to be generated [10]. Combined with the embedded phase tunability and potential amplitude tunability based on variable optical attenuators [15] to dynamically manipulate the optical beams, many future applications can be envisioned, including on-chip lidar, free-space optical communications, object detection, optical trapping, and so on.

This work was funded by the Defense Advanced Research Projects Agency (DARPA) E-PHI and SWEEPER projects, grant no. HR0011-12-2-0007.

## References

- P. F. McManamon, T. A. Dorschner, D. L. Corkum, L. J. Friedman, D. S. Hobbs, M. Holz, S. Liberman, H. Q. Nguyen, D. P. Resler, R. C. Sharp, and E. A. Watson, Proc. IEEE **84**, 268 (1996).

2. N. W. Carlson, G. A. Evans, R. Amantea, S. L. Palfrey, J. M. Hammer, M. Lurie, L. A. Carr, F. Z. Hawrylo, E. A. James, C. J. Kaiser, J. B. Kirk, and W. F. Reichert, *Appl. Phys. Lett.* **53**, 2275 (1988).
3. D. P. Resler, D. S. Hobbs, R. C. Sharp, L. J. Friedman, and T. A. Dorschner, *Opt. Lett.* **21**, 689 (1996).
4. B. Yoo, M. Megens, T. Chan, T. Sun, W. Yang, C. J. Chang-Hasnain, D. A. Horsley, and M. C. Wu, *Opt. Express* **21**, 12238 (2013).
5. B. Yoo, M. Megens, T. Chan, T. Sun, W. Yang, D. A. Horsley, C. J. Chang-Hasnain, and M. C. Wu, in *17th International Conference on Solid-State Sensors, Actuators and Microsystems* (2013), p. 2505.
6. K. Van Acoleyen, H. Rogier, and R. Baets, *Opt. Express* **18**, 13655 (2010).
7. D. Kwong, A. Hosseini, Y. Zhang, and R. T. Chen, *Appl. Phys. Lett.* **99**, 051104 (2011).
8. J. K. Doylend, M. J. R. Heck, J. T. Bovington, J. D. Peters, M. L. Davenport, L. A. Coldren, and J. E. Bowers, *Opt. Lett.* **37**, 4257 (2012).
9. J. Sun, E. Timurdogan, A. Yaacobi, E. S. Hosseini, and M. R. Watts, *Nature* **493**, 195 (2013).
10. J. Sun, D. B. Cole, A. Yaacobi, E. Timurdogan, E. S. Hosseini, G. Leake, D. Coolbaugh, and M. R. Watts, in *Conference on Lasers and Electro-Optics (CLEO)*, 2013, paper CTh5D.1.
11. J. W. Goodman, *Introduction to Fourier Optics* (Roberts & Company, 2005).
12. M. R. Watts, J. Sun, C. DeRose, D. C. Trotter, R. W. Young, and G. N. Nielson, *Opt. Lett.* **38**, 733 (2013).
13. J. Sun, E. Timurdogan, A. Yaacobi, Z. Su, E. S. Hosseini, D. B. Cole, and M. R. Watts, "Large-scale integrated silicon photonic circuit for optical phased array," *IEEE J. Sel. Top. Quantum Electron.* **20** (to be published).
14. P. Dong, W. Qian, H. Liang, R. Shafiiha, D. Feng, G. Li, J. E. Cunningham, A. V. Krishnamoorthy, and M. Asghari, *Opt. Express* **18**, 20298 (2010).
15. J. Liu, M. Beals, A. Pomerene, S. Bernardis, R. Sun, J. Cheng, L. C. Kimerling, and J. Michel, *Nat. Photonics* **2**, 433 (2008).